Structures of Enterococcal Glycerol Kinase in the Absence and Presence of Glycerol: Correlation of Conformation to Substrate Binding and a Mechanism of Activation by Phosphorylatio...

ARTICLE *in* BIOCHEMISTRY · FEBRUARY 2004

Impact Factor: 3.02 · DOI: 10.1021/bi034258o · Source: PubMed

Structures of Enterococcal Glycerol Kinase in the Absence and Presence of Glycerol: Correlation of Conformation to Substrate Binding and a Mechanism of Activation by Phosphorylation†

Joanne I. Yeh,*,‡,§ Véronique Charrier,|| Joao Paulo,‡ Lihui Hou,‡ Emmanuelle Darbon,|| Al Claiborne,⊥ Wim G. J. Hol,@ and Josef Deutscher||

Department of Molecular Biology, Cell Biology and Biochemistry, Brown University, Providence, Rhode Island 02912, Department of Chemistry, Brown University, Providence, Rhode Island 02912, Microbiologie et Génétique Moléculaire, CNRS UMR2585, F-78850 Thiverval-Grignon, France, Department of Biochemistry, Wake Forest University Medical Center, Winston-Salem, North Carolina 27157, and Howard Hughes Medical Institute, University of Washington, Seattle, Washington 98195-7742

Received February 18, 2003; Revised Manuscript Received October 10, 2003

ABSTRACT: The first structure of a glycerol kinase from a Gram-positive organism, *Enterococcus casseliflavus*, has been determined to 2.8 Å resolution in the presence of glycerol and to 2.5 Å resolution in the absence of substrate. The substrate-induced closure of 7° is significantly smaller than that reported for hexokinase, a model for substrate-mediated domain closure that has been proposed for glycerol kinase. Despite the 78% level of sequence identity and conformational similarity in the catalytic cleft regions of the *En. casseliflavus* and *Escherichia coli* glycerol kinases, remarkable structural differences have now been identified. These differences correlate well with their divergent regulatory schemes of activation by phosphorylation in *En. casseliflavus* and allosteric inhibition in *E. coli*. On the basis of our structural results, we propose a mechanism by which the phosphorylation of a histidyl residue located 25 Å from the active site results in a 10−15-fold increase in the activity of the enterococcal glycerol kinase.

Glycerol kinase (GlpK)[1] is a key mediator of glycerol metabolism in bacteria, where it catalyzes the phosphorylation of glycerol to glycerol 3-phosphate (G3P). Glycerol is a ubiquitous molecule, present as a general breakdown product of various metabolic pathways, and is a precursor for the biosynthesis of a variety of important cellular products. As a small, uncharged molecule, glycerol can slowly diffuse across the bacterial membrane, and phosphorylation to G3P traps the molecule in the cytoplasm. This phosphorylation event provides the chemical potential difference for glycerol uptake by creating an imbalance of glycerol concentration across the membrane, in addition to providing a mechanism of regulation. Glycerol uptake is finely coordinated with the transport of PTS sugars, where the presence of these more rapidly metabolized energy molecules suppresses the glycerol uptake system (*1*).

In Gram-positive bacteria such as *Enterococcus*, *Bacillus*, and *Streptococcus*, GlpK is phosphorylated on a histidyl residue (His232 in *Enterococcus*) by HPr, which activates the kinase 10−15-fold. In the Gram-negative glycerol kinase of *Escherichia coli*, regulation occurs via allosteric inhibition through complex formation with enzyme IIA^{Glc}. In both systems, fructose 1,6-bisphosphate (FBP) is an inhibitor of the enzyme (*2*) and has been found to bind to a loop region that in the Gram-positive kinase contains the site of phosphorylation (*3*).

Regulation by proteins of the phosphoenolpyruvate (PEP): sugar phosphotransferase system (PTS), a transport and phosphorylation system for carbohydrates, finely tunes the system so that the most quickly utilized molecules are preferentially transported (*4*, *5*). When PTS sugars are present, the donor of the phosphoryl group to GlpK, HPr, phosphorylates primarily the corresponding sugar-specific enzymes IIA^{Glc}, which in turn phosphorylate the incoming PTS sugars via the appropriate enzymes IIB. However, when the PTS sugars HPr phosphorylates GlpK, activating the kinase which in turn promotes glycerol uptake (*6*). Although glycerol can diffuse across the membrane, glycerol facilitator (GlpF), a membrane channel-forming protein, specifically and efficiently conducts glycerol across the membrane with absolute exclusion of ions and charged solutes (*7*). Earlier studies indicated that the interaction between GlpK with GlpF additionally increases the rate at which glycerol is taken up into the cell (*8*). This may be akin mechanistically to

† This work was supported by March of Dimes Basil O'Conner Grant 5-FY00-564 (J.I.Y.), National Institutes of Health Grant GM/AI-66466 (J.I.Y.), a major equipment grant from the Murdock Charitable Trust to the Biomolecular Structure Center (W.G.J.H.), National Institutes of Health Grant GM-35394 (A.C.), National Science Foundation Grant INT-9400123 (A.C.), and European Union BIOTECH Programme Contract BI04-CT96-0380 (J.D.), the CNRS (J.D.).

* To whom correspondence should be addressed. E-mail: Joanne_Yeh@brown.edu.

‡ Department of Molecular Biology, Cell Biology and Biochemistry, Brown University.

§ Department of Chemistry, Brown University.

|| CNRS UMR2585.

⊥ Wake Forest University Medical Center.

@ University of Washington.

[1] Abbreviations: FBP, fructose 1,6-bisphosphate; GlpK, glycerol kinase; PEP, phosphoenolpyruvate; PTS, PEP:carbohydrate phosphotransferase system; HPr, histidine-containing phosphocarrier protein; enzyme IIAGlc, enzyme IIA glucose; PTS, phosphotransferase system.

10.1021/bi034258o CCC: $27.50
Published on Web 12/18/2003

substrate channeling, where the entering glycerol is immediately shuttled to GlpK for phosphorylation, efficiently creating an imbalance of glycerol concentration across the membrane and promoting uptake. As a key player in mediating glycerol uptake, GlpK is the target of a number of regulatory pathways.

Phosphorylation of GlpK increases its activity (*9*, *10*), although a detailed understanding of how this covalent event promotes catalytic enhancement is largely unknown. Our structures show that transmission of the phosphorylation event would require the signal to be propagated over 25 Å, the distance between the site of phosphorylation (His232) and the active site cleft where glycerol binds. Long-distance intramolecular signal transduction is also necessary in *E. coli* GlpK, as the region of interaction with its allosteric effector, enzyme IIA^{Glc}, is ~30 Å from the catalytic cleft; the response, however, is inhibition rather than activation. Although the structures of *E. coli* GlpK in complex with both enzyme IIA^{Glc} (*11*, *12*) and FBP (*3*) have been published, the mechanism by which inhibition is induced is still largely unknown.

To characterize the conformational changes that accompany substrate binding and phosphorylation to stimulate its activity, we crystallized and determined the structures of GlpK from the Gram-positive bacterium *Enterococcus casseliflavus*, in both the glycerol-bound and unbound forms. No structure of the unbound form from any organism has been determined, so these structural results provide significant new information about the protein-mediated phosphoryl transfer mechanism. Remarkably, the presumed physiologically relevant dimer is nonsymmetric in both the substrate-bound and unbound forms. This nonequivalency of subunits supports a mechanism of signal transduction that involves reorganization of the interaction surfaces between the monomers to transduce the phosphorylation event. The differences that we characterize structurally between the *En. casseliflavus* and *E. coli* GlpKs likely correlate with their respective regulatory mechanisms, providing additional insights into how structure is related to function.

MATERIALS AND METHODS

Complex GlpK. En. casseliflavus GlpK was purified as previously described (*13*) with an additional column step of HighQ, using a Bio-Cad Sprint system. The protein was concentrated to 10 mg/mL and loaded onto the column. After being washed with 8 column volumes (CV) of 20 mM Tris-HCl buffer (pH 7.5), the enzyme was eluted by applying a gradient over 15 CV to 1 M NaCl in Tris-HCl buffer (pH 7.5). The protein eluted as a single peak, at approximately 0.6 M NaCl. Using YM30 centricons, the enzyme was desalted and concentrated and the buffer gradually exchanged with 50 mM Tris-HCl (pH 7.5) in three cycles.

Crystals of GlpK bound with glycerol were obtained from a solution containing 0.1 M sodium acetate buffer (pH 4.5), 6−10% (w/v) PEG 4000, and 10% (w/v) glycerol using a protein concentration of 10 mg/mL at room temperature. This complexed enzyme crystallized in space group $P2_12_12_1$ and with a solvent content of 54%, which results in an occupancy of one dimer per asymmetric unit, with the following cell parameters: $a = 56.95$ Å, $b = 97.35$ Å, and $c = 200.54$ Å. For data collection, all crystals were flash-frozen in a 100 K nitrogen gas stream.

Crystals were screened on an in-house Cu-rotating anode system with an R-Axis II detector, MSC/Yale mirrors, and an MSC cryosystem. Data used for structure determinations were collected at beamlines 7-1 at Stanford Synchrotron Radiation Laboratory, F1 and F2 at Cornell High Energy Synchrotron Source, and X8C at Brookhaven National Laboratory (BNL). All data were processed with Denzo, with Scalepack, and through programs in the CCP4 suite (*14*, *15*).

Despite a level of sequence identity of 55%, molecular replacement (MR) attempts using various approaches (*16*−*19*) with the deposited *E. coli* structures as models were of limited success. The presence of a pseudo-2-fold rotation axis relating the two subunits within the dimer, running parallel to the crystallographic 2-fold screw axis, complicated the Patterson searches. To overcome this problem, heavy atom derivatives were found to obtain additional phasing information by multiple isomorphous replacement (MIR) techniques.

The best heavy atom derivatives were obtained from the lanthanide series metals, particularly of Tb, Yb, and Sm. The lanthanide derivatives had the best phasing statistics but nevertheless amplified the already problematic nonisomorphism exhibited from native crystal to crystal (native differences in R_{sym} of >15%), although not more than any other heavy atom compounds that were tried (Ag, Au, Pt, Pb, and U). To minimize nonisomorphism and improve reproducibility, a procedure of presoaking the crystals in artificial mother liquor containing 15% glycerol for at least 3 h prior to heavy atom soaks helped in reducing differences between crystals. The lanthanide soaks were done for 3−6 h using a 0.5 mM solution; longer soaks at various heavy atom concentrations seemed to increase the degree of nonisomorphism or destroyed the crystals. Data were collected using the in-house Cu-rotating anode on the lanthanide derivatives and the highest-resolution data set diffracted to 3.2 Å (Table 1).

Heavy atom positions were determined using Patterson maps and refined in MLPHARE (*15*). Cross validation using difference Fourier maps, generated with phases calculated from the MR solution, confirmed the four heavy atom positions. These four positions were essentially the same for all the lanthanide derivatives; the strongest solutions refined to occupancies between 0.4 and 1.0, with an overall FOM of 0.52, an R_{cullis} of 0.67, and a phasing power of 1.7 in MLPHARE. Solvent flattening, histogram matching, and gradual phase extension using a higher-resolution native complex data set were carried out in DM (*20*), yielding phase information for σA-weighted map (*21*) generation. From the preliminary maps, ~60% of the Cα backbone could be traced and various regions that were omitted from the model were gradually built in. Iterative cycles of model building of the dimer interface, phosphorylation loop, and enzyme IIA^{Glc}-binding loop and gradual substitution of the native enterococcal sequence were followed by refinement. Iterative cycles of refinement consisting of conjugate gradient minimization, simulated annealing with an initial temperature of 3000 K with 0.5 fs/100 K time steps, and grouped *B*-factor refinement were carried out in X-PLOR/CNS (*16*) using the 2.8 Å native complex data (Table 1). The final complex model with one glycerol bound per monomer subunit and no waters has been refined at 2.8 Å resolution to an R_{free} of 28.2% and an R_{cryst} of 25.1%. In the discussion involving the position of ATP

Table 1: Data Collection and Refinement Statistics

	$GlpK_{native}$ and glycerol (complex)	$GlpK_{native}$ (apo)	GlpK complex, Sm derivative
resolution range (Å)	50−2.8	50−2.5	20−3.2
resolution range in refinement (Å)	6.0−2.8	6.0−2.5	6.0−3.2
total no. of reflections	88774	182355	237112
no. of independent reflections	24267	40746	37997
completeness (%)	87.0	95.3	95.5
completeness at the highest-resolution shell (%)	77.7 (2.93−2.80 Å)	74.7 (2.61−2.5 Å)	91.1 (3.3−3.2 Å)
no. of unique reflections > 3σ	18131	29592	42105
cell parameters (Å)	$a = 57.07$, $b = 97.890$, $c = 200.91$	$a = 56.859$, $b = 97.161$, $c = 201.100$	$a = 57.01$, $b = 97.67$, $c = 201.453$
R_{merge}	8.7	7.2	17.1
R_{cryst}	25.1	22.1	$R_{iso} = 25.7$
R_{free}	28.2	24.3	FOM = 0.52
average B	36.2	34.7	phasing power = 1.7
rmsd for bond lengths (Å)	0.010	0.007	$R_{cullis} = 67\%$
rmsd for bond angles (deg)	1.24	1.2	
rms coordinate error (Å)	0.11	0.10	
no. of protein and substrate atoms (dimer O5−O491, X5−X491)	7240 (one glycerol per monomer)	7228	

Table 2: Se-MAD Data

data set	f''	f'''	resolution limit (Å)	no. of measurements	no. of unique reflections	completeness (%)	$I/\sigma(I)$ (%)	R_{sym} (%)
$\lambda_1 = 0.9791$	−7.560	3.842	2.8	200257	33740	97.5 (98.4)	12.6	9.1
$\lambda_2 = 0.9788$	−6.892	3.839	2.8	198581	33725	97.6 (98.6)	12.4	8.6
$\lambda_3 = 0.954$	−2.818	3.636	2.8	194718	33932	97.8 (98.6)	12.8	8.8

in the glycerol-complexed structure, the position of the nucleotide was modeled on the basis of the *E. coli* structures with ADP bound (*3*, *11*, *22*) and adding the γ-phosphate group, whose bond lengths and angles were positioned according to defined literature values. Our modeling of ATP into the active site of the *En. casseliflavus* complex required no significant remodeling of the active site of the glycerol-complexed structure.

Determination of the exact ncs rotation matrix was achieved through correlation of the positions of ncs-related heavy atom sites. This allowed the ncs pseudo-2-fold axis to be refined. Final confirmation of the dimeric structure came through ncs averaging with DM, and the model was completely traced from the averaged maps except for regions that differed in the two subunits, in particular, the loop regions containing the regulatory histidine and dimer interface regions. The latter regions were traced from nonaveraged, σA-weighted electron density maps.

Apo-GlpK. The His232Ala (H232A) GlpK mutant lacks the site of phosphorylation (activation), although its basal activity is similar to that of the unphosphorylated native enzyme. We used this H232A GlpK mutant for all apo crystal setups, as it yielded diffracting crystals of the apo form. The mutant protein was purified as described for the wild type, and crystals of the H232A GlpK mutant enzyme without substrate (apo) were obtained by hanging drop vapor diffusion, using a protein concentration of 18 mg/mL and from a solution containing 22% PEG 400, 0.1 M potassium phosphate (pH 5.9), and 5 mM 1,10-phenanthroline. Although crystallized under different conditions, the H232A apo-GlpK crystallized in the same space group ($P2_12_12_1$) and with cell dimensions very similar to those of the complex: $a = 56.33$ Å, $b = 95.46$ Å, and $c = 200.53$ Å. Data were collected using the in-house rotating anode source at 100 K to 2.6 Å resolution, with 97% overall completeness. Despite these similarities, MR attempts using the complex as a model did not yield a solution. It was expected that the apo form would be significantly conformationally different from the complex form, possibly in the orientation of domains I and II. Models using just domain I or domain II of the complex structure did not yield a rotation function solution.

On the basis of our previous problems with nonisomorphism in the complex crystals, the SeMet-substituted enzyme was expressed, purified, and crystallized. The SeMet-incorporated enzyme was expressed in methionine auxotrophic strain B834, following standard protocols (*23*), and purified as described for native GlpK, except that 1 mM TCEP was added to the purified enzyme, maintaining a reducing environment. Using the condition found for the crystallization of the H232A apo-GlpK, we were able to obtain data quality crystals of the SeMet-substituted enzyme by microseeding with the unsubstituted H232A apo crystal and growing these at 4 °C, using the same crystallization condition that was used for the unsubstituted H232A apo form, described in detail above. Structure determination was through a three-wavelength multiple anomalous dispersion (MAD) approach, with data collected at 100 K at beamline X8C at BNL with wavelengths of 0.9788 (peak), 0.9791 (inflection), and 0.954 Å (high-energy remote) (detailed statistics listed in Table 2). Three wavelengths were collected, and merging, reduction, and scaling of the data were done in Denzo and Scalepack. Heavy atom positions were found with Solve (*24*), and these positions were iteratively refined. Of the 15 potential selenium sites per monomer, 12 were found and refined to occupancies between 0.6 and 1.0. Initial MAD phases had a figure of merit of 0.68, a phasing power of 1.4, and an R_{cullis} of 71%. Solvent flattening and density modification in Resolve (*24*) yielded initial phasing information, after starting from the experimental MAD phases. At 2.8 Å, the $F_o e^{i\alpha calc}$ maps calculated using the MAD phases clearly showed continuous density for most of the backbone; using each domain from a monomer of the complex structure

E. faecalis	LPKVVSNSEV--YGLTKNY**H**FY**G**SE---VPIAGMAGDQQ
E. casseliflavus	LPEVKSNSEV--YGHTRSY**H**FY**G**SE---VPIAGMAGDQQ
S. aureus	LPEVKASSEV--YGKTIDY**H**FY**G**QE---VPIAGVAGDQQ
S. pyogenes	LPEVKSNSEI--YGKTAAF**H**FY**G**GE---VPISGMAGDQQ
L. lactis	LPEVKSNSEV--YGVTKGF**H**FF**G**SE---VPISGMAGDQQ
B. subtilis	LPEVKPSSHV--YAETVDY**H**FF**G**KN---IPIAGAAGDQQ
L. monocytogenes	LPEVRPSSEV--YADTVPY**H**FF**G**EE---VPVAGIAGDQQ
X. fastidiosa	LPDVRSSSDI--YGLTQTPYF**HG**EQ---IPIAGIAGDQQ
M. pneumoniae	LPKVMPSNAH--FGDIVPS**H**WSTSATGMVPIRGVAGDQQ
M. genitalium	LPKVLSSNAY--FGDIETN**H**WSSNAKGIVPIRAVLGDQQ
M. bovis	LPEIASSAPSEPYGVTLATGPV**G**GE---VPITGVLADQH
M. tuberculosis	LPEIASSAPSEPYGVTLATGPV**G**GE---VPITGVLGDQH
M. leprae	LPAIASSSPLQPYGVTLADGP-**G**GE---VPITGVLGDQH
M. avium	LPEIGPSSSPRPFGVTSDTGPA**GR**---IPITAVLGDQH
C. difficile	LPLVKPSSYV--YGHTDERMLS**GA**K---IPIAGCAGDQQ
C. acetobutylicum	LPEVKNSSEV--YGYTNLGGKG**GI**R---VPIAGMAGDQQ
E. coli	LPEVRRSSEV--YGQTNIGGKG**GT**R---IPISGIAGDQQ
S. typhimurium	LPQVRKSSEV--YGQTNIGGKG**GT**R---IPIAGIAGDQQ
V. cholerae	MPEVKKSSEV--YGQTNIGGKG**GT**R---IPIAGIAGDQQ
H. influenzae	LPEVRNSSEI--YGQTNIGGKG**GV**R---IPVAGIAGDQQ
P. multocida	LPEVRNSSEI--YGQTNIGGKG**GV**R---IPVAGMAGDQQ
Y. pestis	LPEVRPSSEI--YGKTNIGGKG**GT**R---IPIAGIAGDQQ
P. aeruginosa	LPEVRNSSEV--YGNARIGGVG**GG**E---LPIAGIAGDQQ
C. burnetii	LPTVLDNCAQ--FGFTDLDLL-**GHK**---IPITAMIGDQQ
B. pertussis	LPRIAPSSAR--IGETLPEWLG**G**S----IPIAGVAGDQQ

FIGURE 1: Sequence alignment of the regulatory loop carrying the phosphorylatable histidine (H in bold type) in GlpK of Gram-positive bacteria and the FBP binding site in GlpK of Gram-negative bacteria (G and/or R also in bold type). Gram-negative organisms, whose GlpK contains a potentially phosphorylatable histidine, and Gram-positive bacteria, in which a phosphorylatable histidine is absent from GlpK, are underlined.

as a starting model, ~72% of the protein could be placed with major reorientation of domains I and II relative to their orientation in the complex form. Other areas of difference were at the entrance of the catalytic cleft and at the activation loop, as described further in the following section. After initial model building of these regions using the program O (*25*) and initial refinement using the 2.8 Å MAD data, further refinement was done against a higher-resolution 2.5 Å unsubstituted H232A apo data set.

This data set was collected from a crystal of the unsubstituted apo H232A form, crystallized and frozen under the same condition that was used for the SeMet-substituted H232A protein and collected with a wavelength 0.97 Å at beamline X8C at BNL. Initial crystals of apo-GlpK had fairly high mosaicity values (>0.8°) when grown using a hanging drop setup with microliter volumes. Using a nanoscale crystallization approach (*26*), the 2.5 Å diffracting apo crystals had significantly decreased mosaicity values (<0.4°). These crystals exhibited accelerated rates of nucleation and growth, with an approximately 30% reduction in time for nucleations to be first observed. The reduction in mosaicity may be due to the concomitant reduction in the extent of oxidation, deamidation, or other degradating reactions that become more significant with time and can increase nonhomogeneity in the protein so that an enhanced rate of equilibration can exert an overall positive effect on crystal formation and growth.

Refinement of the structure was achieved with CNS, as described earlier for the complex structure. Both σA-weighted and Resolve maps were generated to assess the model after every round of refinement. The final H232A apo model has been refined to 2.5 Å to an R_{free} of 24.3% and an R_{cryst} of 22.1% (Table 1), without waters.

The refined, cross-validated (*27*, *28*) structures of the H232A apo-GlpK and wild-type (WT) complex GlpK were analyzed through superpositioning and difference-distance matrices to quantitate structural differences (*29*).

RESULTS AND DISCUSSION

General Structural Features. A subunit of the *En. casseliflavus* GlpK is composed of two domains with a topology similar to that of the ATPase core of hexokinase (*30*). The interface of the two domains forms the catalytic cleft in which glycerol and ATP bind (Figure 2A,B), and this region is entirely conserved in the sequence and structural motif of the *En. casseliflavus* and *E. coli* enzymes. Located approximately 25 Å from the catalytic cleft, at the interface of the *En. casseliflavus* GlpK dimer, is the loop that contains a conserved histidine, His232 (Figure 1). In contrast to the highly conserved catalytic cleft, the amino acid sequence and structure at the regulatory regions are significantly different in the GlpK enzymes from *En. casseliflavus* and *E. coli*.

The active oligomer is a dimer, and the two subunits are nonequivalent structurally although identical in sequence. Particularly significant differences occur in two subregions of domain I: (i) at the dimer interface (denoted as "I-int" in the text and figures) comprising residues 5−78 extending from the N-terminus and (ii) at the loop containing the phosphorylatable histidine ("I-phos") comprising residues 225−240 (Figure 2A). These subregions differ by an rms value of 2.4 Å in the O and X subunits with larger differences for certain residue pairs, whereas the catalytic cleft and contiguous regions exhibit much smaller rms differences of only 0.6−0.8 Å over 300 Cα atoms.

En. casseliflavus GlpK appears to form a pseudotetramer in the $P2_12_12_1$ crystals that are obtained (Figure 3A). Two equivalent dimers are formed, one by subunits O and X and the second by subunits Y and Z, following the nomenclature introduced by Hurley et al. (*11*). (It should be noted that our discussions of the O−X dimer also apply to the Y−Z dimer, which is equivalent, although for the sake of brevity, only the O−X dimer will be denoted.) These dimers are positioned in the crystal in such a way that significant contacts occur between subunits O and Y but none between

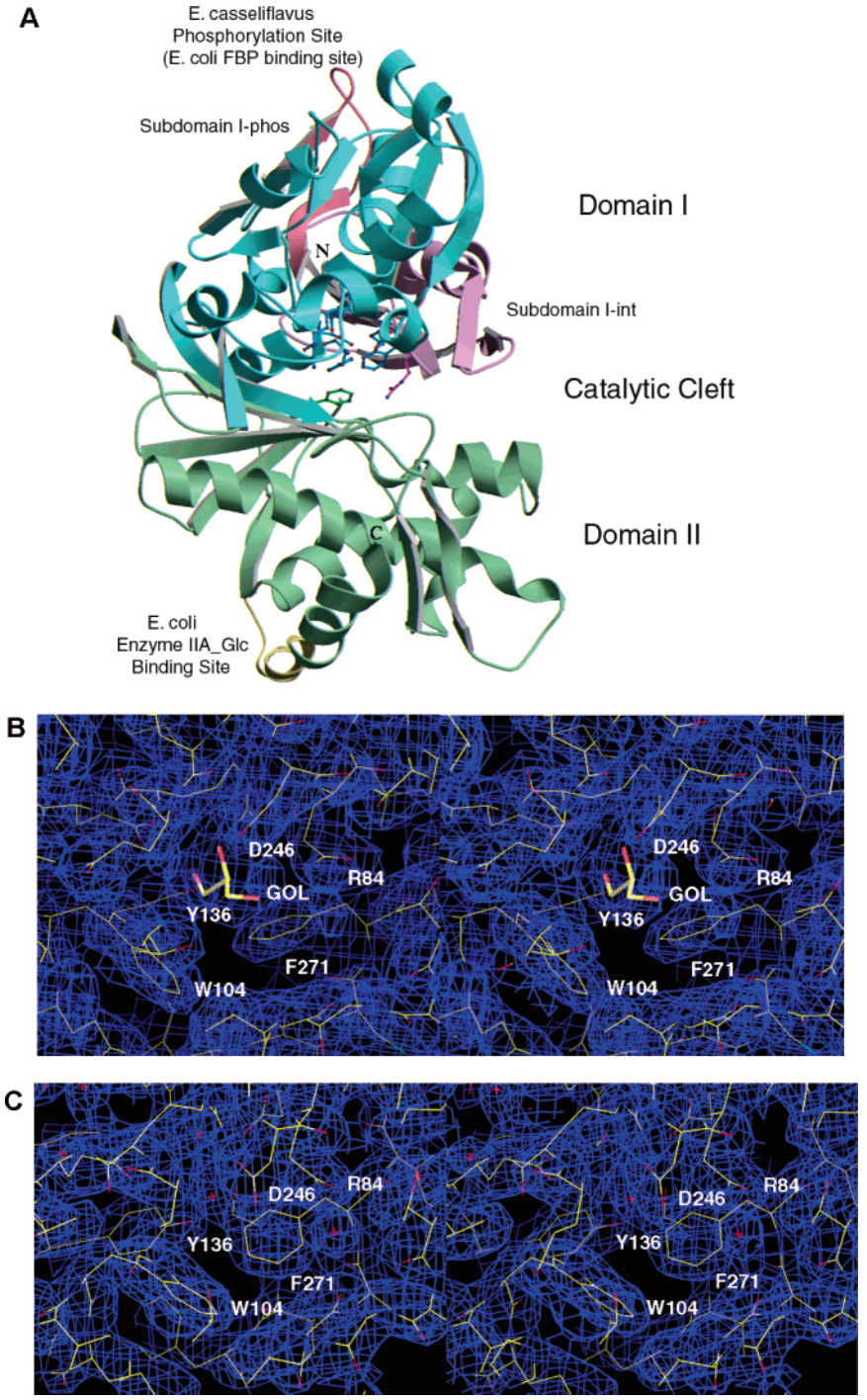

FIGURE 2: (A) Ribbon representation of a monomer of GlpK. Domains and "subregions" are highlighted by a different color as follows: domain I in cyan, domain II in green, subregion I-int in purple, and subregion I-phos in red. The catalytic cleft is at the interface of the two domains, I and II, and glycerol binds deep within the catalytic cleft. The residues that interact with glycerol are depicted in ball-and-stick representation and colored according to their respective domains. Subregion I-int, comprised of residues 5−78, includes the interface helix of the O−X dimer, while subregion I-phos, comprising residues 225−240, includes the activation loop. These regions differ the most between the O and X subunits within the dimer. The regulatory regions of both the *En. casseliflavus* and *E. coli* GlpK enzymes are distal from the catalytic cleft. In *En. casseliflavus*, the loop that contains the phosphorylation site, His232 (shown in red), is approximately 25 Å from the catalytic cleft; this is the same region that binds FBP in *E. coli*. In *E. coli*, the region of the kinase that interacts with enzyme IIA^{Glc} (shown in yellow) is ~30 Å away. (B and C) Stereoview of the σ_A-weighted $2|F_o - F_c|$ electron density maps contoured at 3.5σ of the complex (B) and apo (C) substrate binding sites, where the residues that interact with the glycerol substrate are labeled. This figure was created with the program O (*23*).

subunits X and Z (Figure 3A). This is in distinct contrast to *E. coli* GlpK, where the tetramer has exact 222 point group symmetry and subunit contacts are equivalent (Figure 3B). The subunits within the O−X dimer of *En. casseliflavus* GlpK are related by a pseudo-2-fold axis of 177.3° which runs parallel to the crystallographic 2_1-screw axis. As discussed later, this nonequivalence may be ultimately related to the mechanism of signal transduction that communicates the phosphorylation event from the distal loop to the catalytic site.

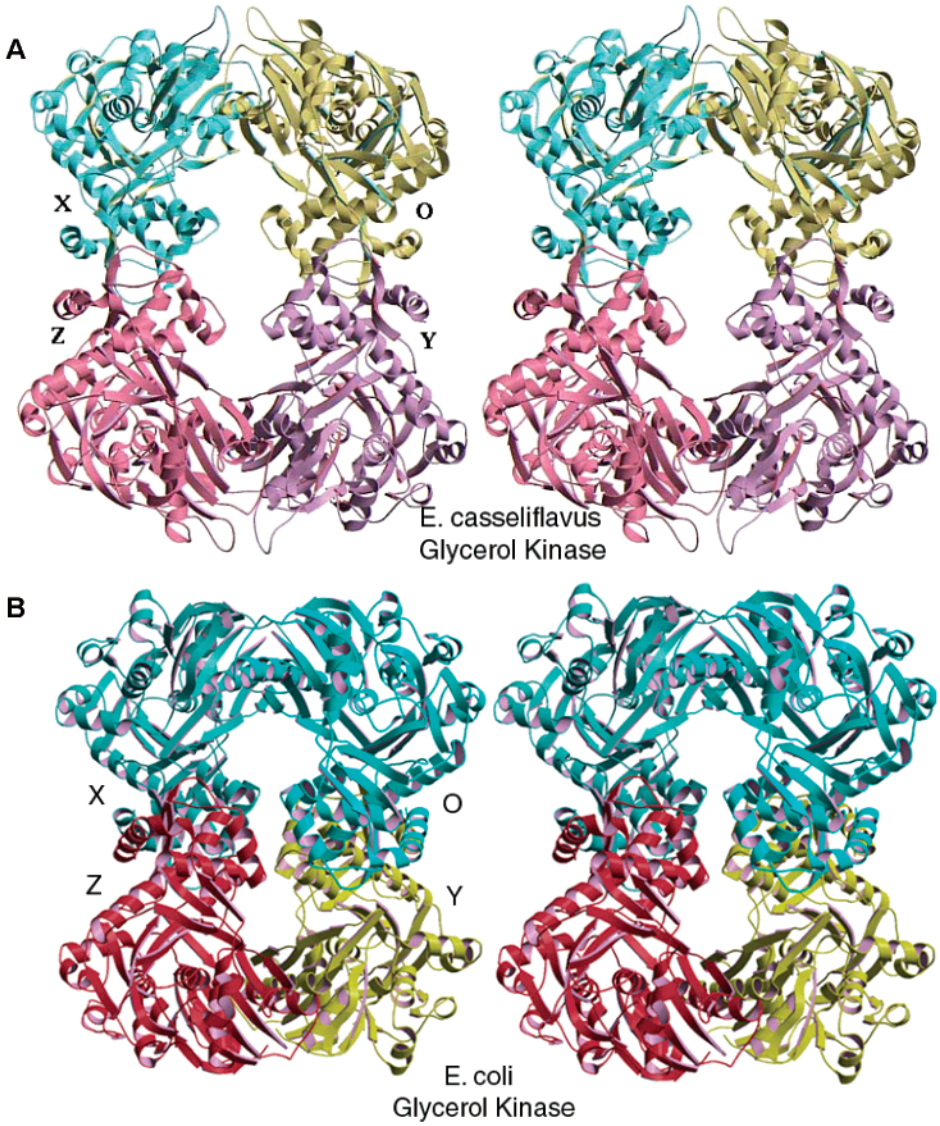

FIGURE 3: Stereo figures of the packing in the *En. casseliflavus* (A) and *E. coli* (*11*) (B) GlpK crystals. Each monomer is differentiated by a separate color, and each subunit is denoted as O, X, Y, or Z (*11*). In *En. casseliflavus* GlpK, a rotation of the top dimer (O−X) relative to the bottom dimer (Y−Z) differentiates the packing from that of an exact tetramer, with no contacts between the X and Z subunits. In *E. coli* GlpK, the packing is tetrameric with exact 222 point group symmetry.

In the *En. casseliflavus* GlpK structure, the O−X dimer buries 2300 Å^2, due largely to the intimate interactions concentrated near the loop region containing the regulatory histidine His232. This loop region is composed of residues 225−240 of both the O and X subunits. Additional contacts occur between the long interface helices, encompassed by residues 49−68, forming a coiled-coil pair. These extensive contact regions indicate that the globular O−X dimer is most likely the physiologically relevant form of *En. casseliflavus* GlpK. The O−X dimer is also thought to be the entity recognized by P∼His-HPr for phosphorylation.

Conversely, in the *E. coli* GlpK structure, the O−X dimer buries only 400 Å^2 and is not thought to be the catalytically competent dimer (*11*). For *E. coli* GlpK, there was speculation that the elongated O−Y dimer is the physiologically relevant oligomer, with a buried surface area of 3400 Å^2. In contrast, the *En. casseliflavus* O−Y dimer buries only 1700 Å^2, half that of the *E. coli* O−Y dimer and less than that of the O−X form of the *En. casseliflavus* enzyme. Moreover, there is no contact between the X and Z subunits in the *En. casseliflavus* GlpK pseudotetramer (Figure 3A).

Additional evidence of differences at the regulatory domains of *E. coli* GlpK can be obtained from the interactions of the allosteric effectors fructose 1,6-bisphosphate (FBP) and enzyme IIA^{Glc}. Both of the effector molecules bind to specific regions located ∼25−30 Å from the catalytic cleft on opposite sides of the GlpK molecule. In contrast, GlpK of Gram-positive bacteria does not interact with enzyme IIA^{Glc}, but becomes phosphorylated at a histidyl residue in a PEP-dependent reaction catalyzed by enzyme I and HPr, the two general proteins of the PTS, as described earlier. Interestingly, the FBP binding loop of *E. coli* GlpK corresponds to the loop containing the phosphorylatable histidine in the *En. casseliflavus* enzyme. However, FBP binding to *E. coli* GlpK and phosphorylation at His232 of the *En. casseliflavus* enzyme exert antagonistic effects on GlpK activity, and the conformations of these regions are significantly different in the two enzymes. The *En. casseliflavus* activation loop is in an extended conformation, whereas the *E. coli* loop is "closed down" and symmetrical (Figure 4). This extension of the loop from the surface of the protein in *En. casseliflavus* may facilitate phosphorylation

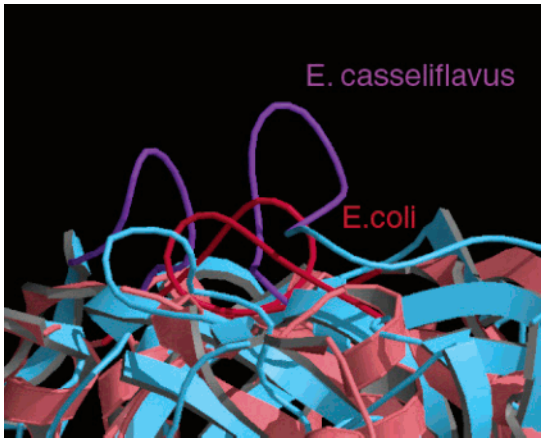

FIGURE 4: Significant differences exist between the *E. coli* and *En. casseliflavus* oligomers, and these differences are especially pronounced at the regulatory regions. The activation loop region of *En. casseliflavus* is well-ordered, while this loop is structurally ordered only with the binding of the inhibitor, FBP, in *E. coli*. In *En. casseliflavus*, these loops are extended, possibly enhancing the accessibility of these regions to HPr for phosphorylation, in contrast to the *E. coli* loop conformation.

by HPr during activation of the enzyme by providing greater accessibility to the histidine.

Apo and Glycerol-Complexed Forms and the Catalytic Cleft. Glycerol binds deep within the catalytic cleft (Figure 2A) with hydrogen bonding interactions with residues Arg84, Trp104, Tyr136, and Asp246. The electron density maps provide clear indications of the presence and absence of glycerol in the complex and apo structures (Figure 2B,C). Minor structural differences are found when the catalytic cleft and contiguous regions of each of the subunits in the dimeric *En. casseliflavus* GlpK complex (with glycerol) are compared to those of the *E. coli* GlpK complex (with glycerol, ADP, and enzyme IIAGlc). In the O−X dimer, rms deviations of 0.6 and 0.8 Å are found, respectively, for 315 Cα atoms out of a total of 487 Cα atoms per monomer subunit (omitting the interface helix, enzyme IIA^{Glc}-binding, and loop regions). As a consequence, the catalytic clefts are essentially the same: the positions of glycerol and active site residues are superimposable. This structural similarity reflects the conservation of substrate-binding motifs near the catalytic site and the high degree of sequence identity of this region between GlpKs from Gram-positive and Gram-negative bacteria (Figure 1). Hence, it appears that the active site region in GlpK enzymes from these divergent organisms is genetically and structurally conserved, whereas striking differences exist in other parts of the enzyme, correlating to the differing regulatory mechanisms that are operating in the Gram-positive and Gram-negative systems.

The active site cleft accommodates two substrates, glycerol and ATP, the phosphoryl group donor. ADP has been shown to bind close to the entrance of the cleft and introduced no additional conformational changes in the *E. coli* GlpK−glycerol complex (*11*, *12*, *31*). The binding of this nucleotide substrate is expected to be conserved, as described above.

Considerable changes in the orientation of domains I and II occur when the apo subunit is compared to the complex. These differences can be described as a rotation about an axis that is on the periphery of the monomer, close to the glycerol binding site (Figure 5). Using the entrance of the catalytic cleft site as the reference, glycerol binds deep in the cleft whereas ADP binds near the opening. The region closest to the glycerol binding site exhibits localized changes of side chain orientations but no significant backbone conformational changes, indicating that the site is essentially "primed" for glycerol binding.

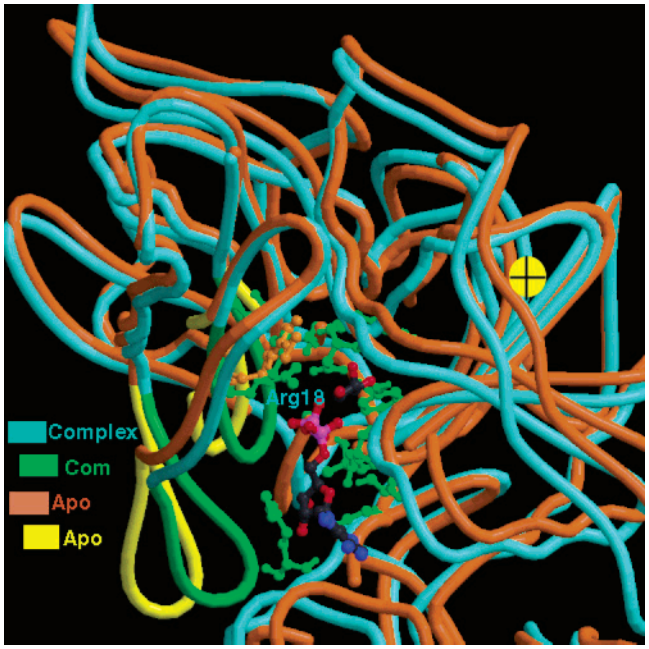

FIGURE 5: Superposition of the *En. casseliflavus* apo (orange) and complex (cyan) monomer subunits viewed down the axis of rotation (denoted with a yellow, cross-marked circle). Conformational differences are found at the entrance of the catalytic cleft, where the binding of substrates results in a significant reduction in solvent accessibility. Two loop regions, highlighted in green (complex) and yellow (apo), near the opening of the catalytic cleft exhibit especially pronounced changes and close off the entrance of the active site after substrate binding. Possibly related to the mechanism of catalysis is the movement of the loop that includes Arg18. This arginine may be especially important in phosphoryl transfer, and the conformational changes observed upon binding of glycerol may help to position Arg18 closer to the γ-phosphate of ATP to enhance phosphoryl transfer to glycerol.

In contrast, the region around the entrance of the catalytic cleft exhibits the greatest changes in conformation whereby the active site becomes closed off to prevent solvent or other molecules from entering once both substrates are bound. Particularly striking are changes at two loop regions at the opening of the cleft, encompassed by residues 9−19 and 36−48 (Figure 5). Especially relevant may be the change in the loop of residues 9−19 as Arg18 may be a key residue in mediating transfer of a phosphoryl group from ATP to glycerol. The movement of the loop brings Arg18 closer to the nucleotide-binding region, supporting the idea that Arg18 may aid in shuttling the phosphoryl group from ATP to glycerol.

This domain closure is reminiscent of that exhibited by hexokinase, although the overall magnitude of rotation of 7° is appreciably smaller than the rotation of 12° observed for hexokinase. The resulting atomic movements of the polypeptide backbone can be as much as 5.5 Å, in those regions farther away from the point of rotation. The overall root-mean-square deviation of the apo and glycerol-complexed forms is 2.7 Å over 471 Cα atoms. The glycerol-induced domain closure, in conjunction with the surface area that becomes buried by the substrate, drastically reduces the

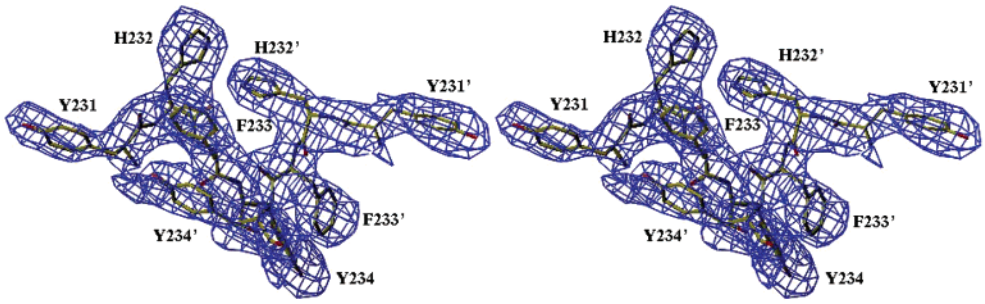

FIGURE 6: Stereoview of a figure-of-merit-weighted F_{obs} electron density map for *En. casseliflavus* Glp*K* contoured at 1σ of the loop region containing the phosphorylation site from residue 231 to 234 of both O and X subunits. Residues denoted with primes are from the O subunit. The electron density is well-defined in this region, in contrast to that in *E. coli* GlpK where this region could not be traced due to disorder. The aromatic residues clustered at this region may function in recognition of the phosphorylation site by HPr.

solvent accessibility of the catalytic cleft by ~62%. Once the effect of ATP (ADP) binding is included, the accessibility is reduced by an additional 12%, leaving only 26% of the initial enzyme surface solvent accessible. This reduction in solvent accessibility suggests that ATP binding must follow immediately upon glycerol binding since the closure of the binding cleft would preclude most molecules from entering the active site once glycerol is fully bound and conformational closure is completed.

The smaller magnitude of the conformational change between the apo and glycerol-complexed forms for GlpK compared to hexokinase could be a consequence of the three-carbon, three-oxygen substrate that is accommodated at the active site relative to the larger six-carbon, six-oxygen substrate in hexokinase. Related to this question of how the conformational changes can be correlated to the mechanism catalyzed by the kinase is how the phosphorylation of a histidine at a distance of 25 Å is propagated to the active site to enhance this rate of reaction.

Intramolecular Signal Transduction and the Phosphorylation Loop. When *E. coli* GlpK was crystallized in the presence of glycerol and ADP or in a quaternary complex additionally containing the allosteric effector enzyme IIA^{Glc}, the loop corresponding to the *En. casseliflavus* GlpK activation loop could not be traced due to disorder (*11*). Interestingly, in *E. coli* GlpK complexed with glycerol and the allosteric effector FBP, this loop was stabilized and was found to be the binding site for the inhibitor (*3*). One FBP molecule is bound to the O−X dimer and one to the Y−Z dimer in an asymmetric manner. Gly235 and Arg237 from each subunit bind the glycolytic intermediate, thus favoring dimer−tetramer association. As can be seen from panels A and B of Figure 3 and from Figure 4, there are structural differences between the FBP binding loop in GlpK of *E. coli* and the activation loop of GlpK from *En. casseliflavus*.

Despite the 77% level of overall sequence similarity between *En. casseliflavus* and *E. coli* GlpKs, the amino acid sequences of the activation loop in GlpK of Gram-positive bacteria and of the FBP binding loop in GlpK of Gram-negative organisms are completely different (Figure 1). The FBP binding loop contains several Gly residues and a Lys residue and exhibits similarity in structure and sequence to the Walker A motif (P-loop) of nucleotide binding proteins (*3*). In contrast, the phosphorylatable histidine in GlpK of Gram-positive bacteria is surrounded by three conserved aromatic amino acids (either Tyr or Phe), which form a hydrophobic patch near the base of the activation loop. In the GlpKs of most Gram-negative bacteria, these residues are glycine or lysine, whereas these aromatic residues are conserved in Gram-positive bacteria (Figure 1). However, *E. coli* GlpK in complex with FBP indicates that the tetramer may "sequester" the enzyme in an inactive state, suggesting that the dimer is the active oligomer, responsible for catalytic function in both bacterial systems (*3*, *22*).

In the *En. casseliflavus* GlpK, the loop containing His232, which becomes reversibly phosphorylated to activate the kinase, is well-ordered in both subunits (Figure 6). This activation loop lies approximately 25 Å away from the catalytic cleft at an interface of the O−X dimer. This brings the histidines from the O and X subunits to within 5 Å of each other. The stoichiometry of phosphorylation is likely two per dimer so that each histidine in both subunits becomes phosphorylated in GlpKs of most Gram-positive bacteria. Evidence for this assumption has been obtained from measurements of the levels of phosphorylation in GlpK from *Enterococcus faecalis* (*13*) and *Bacillus subtilis* (*32*), where ~90% of the molecules were found to carry a phosphoryl group after incubation with PEP, enzyme I, and HPr. In addition, in *En. faecalis* cells cultured in the presence of glycerol, up to 85% of the GlpK molecules were present in their phosphorylated form (*9*). The proximity of the two His232 residues in the active dimer of *En. casseliflavus* GlpK suggests that phosphorylation at both histidines is likely to cause significant conformational changes due to charge-repulsion effects, propagating a signal of the phosphorylation event (Figure 7).

This signal could be further propagated through rearrangement of the dimer interface helices (I-int in Figure 2), as the interaction of these structural elements can be facilely changed without requiring a large change in the overall conformation of the monomer subunit. The interface subregion lies at the periphery of the glycerol-binding cleft and is involved in binding ATP, as described earlier (Figure 5). In the structure of *E. coli* Glp*K* with glycerol and ADP bound, one residue in particular appears to be important for regulating catalysis: Arg17 (Arg18 in *En. casseliflavus* GlpK) interacts with both the O2 and O3 atoms of the β-phosphate moiety of ADP (*11*). This arginine residue is conserved in both Gram-positive and Gram-negative GlpKs. When the O and X subunits of the *En. casseliflavus* GlpK−glycerol complex and the *E. coli* GlpK−glycerol−ADP complex are compared, the position of the guanidinium group differs by up to 3 Å. This suggests that conformational changes of subregion I-phos, resulting from phosphorylation

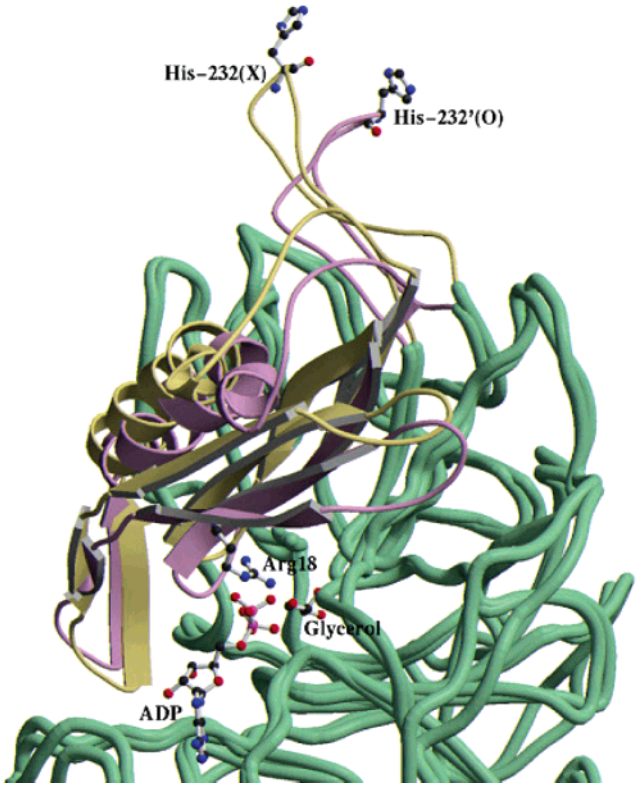

FIGURE 7: Superposition of the X subunit onto the O subunit of the *En. casseliflavus* O−X dimer. Large portions of the monomers are similar with rms deviations of 0.6−0.8 Å at the contiguous regions surrounding the catalytic cleft (300 Cα atoms). These regions are shown as green coils in both subunits. The largest regions of difference are localized to subregions I-int and I-phos. These regions are represented as strands, helices, and loops and colored purple for the O subunit and yellow for the X subunit. As depicted in this figure, changes at the loop region may be transmitted to the catalytic cleft by the interface helices, in particular to Arg18. Arg18 and glycerol from the *En. casseliflavus* X subunit are shown, and ADP is modeled from the *E. coli* structure (*11*).

of His232, may induce subsequent changes in subregion I-int. This would ultimately reposition Arg18, which would be brought into a more optimized geometry for mediating the phosphoryl transfer of the γ-phosphate group of ATP to glycerol through the formation of a transient phosphoenzyme intermediate.

Although this change is propagated through several residues, altering the position of Arg18 may be particularly important since phosphorylation is known to affect k_{cat} (the rate of turnover) but not K_m (the binding affinity) (*9*). The changes observed in these structures support a model in which the binding affinity for ATP is unaffected but the rate of transfer of a phosphoryl group from ATP to glycerol is enhanced (*9*, *13*). Adjusting the position of Arg18 could have exactly such an effect, by affecting the conformation of this residue for transition-state stabilization during phosphoryl transfer in the active site, enhancing the activity by more than 10-fold.

Prior to our current results, a model of the conformational change that accompanies glycerol binding was largely based on hexokinase (*30*, *33*). However, our results suggest that the mechanism of phosphoryl transfer is mediated by an intermediate state whereby the enzyme shuttles the γ-phosphoryl group from ATP to glycerol. In contrast, hexokinase, and possibly the *E. coli* GlpK, which is not regulated by an

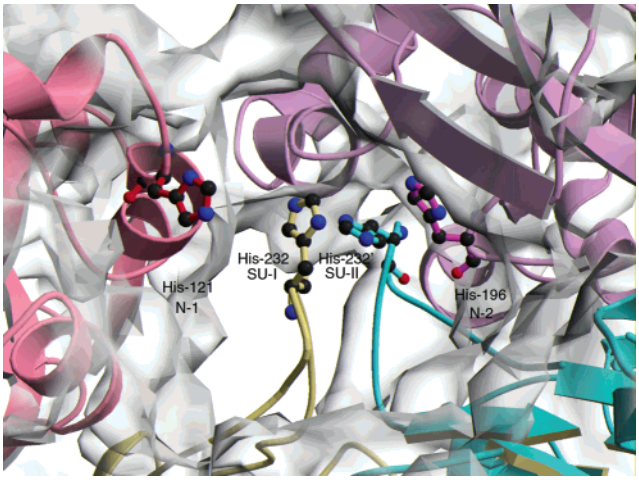

FIGURE 8: Stereoview of the "histidine chain" found at the activation loop region, formed by regulatory histidines His232′ and His232 of the O−X dimer and histidines His121 and His196 from symmetry-related O (in red) and X (in purple) subunits. These additional molecular interactions may suggest how molecules of GlpK can be sequestered for molecular recognition.

enzyme phosphorylation−activation mechanism, appear to follow a sequential reaction where the phosphoryl group is transferred directly between substrates with "in-line" geometry that results with an inversion of configuration at the phosphorus atom (*34*).

Another indication that phosphorylation of the distal loop results in a conformational change that is propagated to enhance catalysis is the location of the binding site of the negative effector, FBP. As discussed earlier, this binding site has been shown to be at the interface of the O−X dimer loops of *E. coli* GlpK (*3*). FBP exerts a similar inhibitory response in *En. casseliflavus* GlpK (*13*). This could be achieved by preventing the requisite conformational change of the loops that ultimately results in the reorientation of the active site residue(s) to enhance catalysis. This would sequester the enzyme in the less catalytically active structural form and provides additional evidence supporting our proposed mechanism for activation of the enzyme.

MOLECULAR RECOGNITION

Both activation loops of the O−X dimer are engaged in crystal contacts such that each His232 has a nearby histidine from a symmetry-related molecule which forms a chain of histidines at the interface (Figure 8). Specifically, His121 of one GlpK molecule comes within 5.5 Å of His232 of the X subunit, and His196 from another GlpK molecule is situated near His232 of the O subunit. Although the locations of these residues are due to crystal packing, these nearby His121 and His196 residues may indicate alternative conformations for the donating phosphorylated histidine from HPr, especially as they are in an orientation that appears to be well-suited for donator−acceptor interactions. In conjunction with the aromatic residues clustered at this site, the patch of histidines may function in the recognition of sites of phosphorylation in GlpK. The transient association of multiple molecules of GlpK for recognition and enhancement of the phosphoryl transfer reaction may present a plausible scenario of a mechanism of molecular recognition.

Interestingly, HPr employs a similar paradigm of interacting hydrophobic surfaces which includes residues Ile47,

Met48, Val50, and Met51 in binding to its different partners: glycogen phosphorylase, enzyme I, and enzyme IIA^{Glc} (*35*). Hydrophobic surfaces in the vicinity of the phosphorylatable histidine are present also in enzyme I and enzyme IIA^{Glc}, and these regions have been implicated in interactions with HPr (*36*, *37*). It is therefore likely that a similar recognition scheme is utilized in most Gram-positive GlpKs, where the hydrophobic "interaction" patch from HPr makes contact with the patch of aromatic amino acids surrounding the phosphorylatable histidines in the GlpK dimers (Figure 6).

Enzyme IIAGlc Binding Region in E. coli GlpK. The GlpK−enzyme IIA^{Glc} complex determined by Hurley et al. (*11*) showed that the regulatory protein binds at one end of GlpK, approximately 30 Å from the catalytic cleft and opposite the FBP binding loop, which corresponds to the activation loop containing His232 in *En. casseliflavus* GlpK (Figure 2A). The interaction of enzyme IIA^{Glc} with *E. coli* GlpK is primarily through residues in a helical region, comprising residues 470−481, close to the C-terminus. This region of *E. coli* GlpK is structurally disordered prior to binding of enzyme IIA^{Glc} and becomes an ordered helix after binding (*11*). In contrast, in the *En. casseliflavus* enzyme, the electron density in this region is well-ordered, despite the lack of interaction with effector proteins. No interactions seem to occur between *En. casseliflavus* GlpK and enzyme IIA^{Glc}, since the PTS protein from either Gram-positive or Gram-negative bacteria exerted no effect on *En. casseliflavus* GlpK activity (*13*). Thus, although regulation of glycerol kinase by PTS proteins in Gram-positive and Gram-negative bacteria is mediated by very different mechanisms, both systems rely on long-range effects to modulate enzyme catalysis.

CONCLUSIONS

The structures of the *En. casseliflavus* apo and complex GlpK forms provide an enhanced understanding of the mechanism of catalysis employed by this key enzyme in the glycerol metabolism pathway. These structural results provide additional new insights into the effects of several *glpK* mutations, which permitted the Gram-positive *B. subtilis ptsHI* mutants to grow on glycerol as the sole carbon source (*38*).

Due to the absence of GlpK phosphorylation, *B. subtilis ptsHI* mutants are normally unable to metabolize glycerol efficiently (*5*, *39*, *40*). However, several pseudorevertants could be isolated which had regained the capacity to utilize glycerol and which all had *glpK* mutations (*38*). Only one mutation affected an amino acid in the catalytic cleft, that of a Phe135Ser mutant, and this result is likely due to the proximity of this residue to the key Tyr134 (Tyr136 in *Enterococcus*) residue that participates in glycerol binding. More significantly, two other mutations affected amino acids in the activation loop located at the interface of the O−X dimer (Figure 3A). In one mutant, the phosphorylatable His230 in *B. subtilis* GlpK was replaced with an arginine; in the other, the neighboring Phe232 was exchanged for a serine. These two mutations likely caused structural changes similar to those resulting from phosphorylation at His230 of *B. subtilis* GlpK. In agreement with this assumption, *En. casseliflavus* H230R (*13*) and *B. subtilis* H232R (*32*) mutant GlpKs exhibited elevated activity similar to that observed for phosphorylated GlpKs. It is likely that electrostatic repulsion caused by the two positively charged arginines located in neighboring activation loops in the mutant GlpK O−X dimer leads to structural changes similar to those caused by the negative charges of the phosphoryl groups bound to the Nϵ2 position of His232. As already discussed, *in-vitro* and *in-vivo* experiments showed that the regulatory histidines in both subunits of the O−X (Y−Z) dimer become phosphorylated (*10*, *13*, *32*).

Another key mutant led to enzyme I- and HPr-independent GlpK activity; this was a Glu65Gly substitution (*38*). This amino acid is located in the coiled-coil pair of subunit interaction helices in the center of the O−X dimer. These helices in our model of intramolecular signal transduction propagate the phosphorylation event at His232 to the active site to reorient specific residues. This replacement of a Glu with a Gly residue likely affected the conformation of the residues at the periphery of the active site, in particular Arg18, whose orientation may be essential for efficiently mediating transfer of a phosphoryl group from ATP to glycerol, as discussed earlier. This Glu65Gly mutant may have a conformation that locks the subunit helices, and consequently Arg18, into a more optimal conformation.

Conservation of Glu65, His230, and Phe232 residues occurs only in GlpKs of Gram-positive, but not Gram-negative, bacteria, suggesting that they have a specific function in regulating GlpK activity in the former organisms. However, Phe135 in the catalytic cleft is conserved in GlpKs from both types of bacteria. The effects of mutations of these residues again highlight the molecular and mechanistic themes that have been correlated to the GlpK structures described in this report: conservation of binding and catalytic motifs with divergences in regulatory interactions. Because of slow hydrolysis of the phosphoamidate bond in P∼GlpK, it will be very difficult to study the structural effect of phosphorylation directly with a crystal structure of P∼GlpK. It will therefore be interesting to determine the structure of one or several mutant GlpKs exhibiting elevated activity probably because of structural changes similar to those caused by phosphorylation.

Our model of a ternary complex of ATP, glycerol, and GlpK shows that the phosphorus atom of the γ-phosphate is 4.5 Å from the 3-hydroxyl of glycerol. This distance does not preclude a dissociative mechanism for transfer of a phosphoryl group to the 3-hydroxyl. However, we favor a phosphoryl transfer mechanism that is mediated through the enzyme, and this model aptly links our structural results with the reported K_m and k_{cat}. Our model of intramolecular signal transduction from the site of phosphorylation, necessitating propagation of the covalent event over 25 Å, is through rearrangement of helical elements to precisely position Arg18 at the active site and again ties our structural results with biochemical analysis. Our models are likely generally applicable to other enzymes utilizing long-range regulatory mechanisms based on phosphorylation.

ACKNOWLEDGMENT

Data were collected at the Stanford Synchrotron Radiation Laboratory, Cornell High Energy Synchrotron Source, and Brookhaven National Laboratory. We thank all the staff for

their assistance, particularly Dr. Li-Wei Hung at BNL for his technical expertise.

SUPPORTING INFORMATION AVAILABLE

A movie depicting the proposed two-part intramolecular signal transduction mechanism is available. The first involves a rotation of domains I and II to close off the active site upon substrate binding. The second models the conformational change that would follow phosphorylation of the histidines at the loop region. This change is propagated through the dimer interface helices and ultimately repositions Arg18 to more optimally mediate transfer of a phosphoryl group from ATP to glycerol. This material is available free of charge via the Internet at http://pubs.acs.org.

REFERENCES

1. Saier, M. H., Jr., and Roseman, S. (1976) Sugar transport. Inducer exclusion and regulation of the melibiose, maltose, glycerol, and lactose transport systems by the phosphoenolpyruvate:sugar phosphotransferase system, *J. Biol. Chem. 251*, 6606−6615.
2. Lin, E. C. (1976) Glycerol dissimilation and its regulation in bacteria, *Annu. Rev. Microbiol. 30*, 535−578.
3. Ormö, M., Bystrom, C. E., and Remington, S. J. (1998) Crystal structure of a complex of *Escherichia coli* glycerol kinase and an allosteric effector fructose 1,6-bisphosphate, *Biochemistry 37*, 16565−16572.
4. Gay, P., Cordier, P., Marquet, M., and Delobbe, A. (1973) Carbohydrate metabolism and transport in *Bacillus subtilis*. A study of *ctr* mutations, *Mol. Gen. Genet. 121*, 355−368.
5. Reizer, J., and Peterkofsky, A. (1987) Regulatory mechanisms for sugar transport in gram-positive bacteria, in *Sugar transport and metabolism in Gram-positive bacteria* (Reizer, J., and Peterkofsky, A., Eds.) pp 333−364, Ellis Horwood, Chichester, U.K.
6. Romano, A. H., Saier, M. H., Jr., Harriott, O. T., and Reizer, J. (1990) Physiological studies on regulation of glycerol utilization by the phosphoenolpyruvate:sugar phosphotransferase system in *Enterococcus faecalis*, *J. Bacteriol. 172*, 6741−6748.
7. Fu, D., Libson, A., Miercke, L. J. W., Weitzman, C., Nollert, P., Krucinski, J., and Stroud, R. M. (2000) Structure of a Glycerol-Conducting Channel and the Basis for Its Selectivity, *Science 290*, 481−486.
8. Voegele, R. T., Sweet, G. D., and Boos, W. (1993) Glycerol Kinase of *Escherichia coli* is Activated By Interaction with the Glycerol Facilitator, *J. Bacteriol. 175*, 1087−1094.
9. Deutscher, J., and Sauerwald, H. (1986) Stimulation of dihydroxyacetone and glycerol kinase activity in *Streptococcus faecalis* by phosphoenolpyruvate-dependent phosphorylation catalyzed by enzyme I and HPr of the phosphotransferase system, *J. Bacteriol. 166*, 829−836.
10. Deutscher, J., Bauer, B., and Sauerwald, H. (1993) Regulation of glycerol metabolism in *Enterococcus faecalis* by phosphoenolpyruvate-dependent phosphorylation of glycerol kinase catalyzed by enzyme I and HPr of the phosphotransferase system, *J. Bacteriol. 175*, 3730−3733.
11. Hurley, J. H., Faber, H. R., Worthylake, D., Meadow, N. D., Roseman, S., Pettigrew, D. W., and Remington, S. J. (1993) Structure of the regulatory complex of *Escherichia coli* III^{Glc} with glycerol kinase, *Science 259*, 673−677.
12. Feese, M., Pettigrew, D. W., Meadow, N. D., Roseman, S., and Remington, S. J. (1994) Cation-promoted association of a regulatory and target protein is controlled by protein phosphorylation, *Proc. Natl. Acad. Sci. U.S.A. 91*, 3544−3548.
13. Charrier, V., Buckley, E., Parsonage, D., Galinier, A., Darbon, E., Jaquinod, M., Forest, E., Deutscher, J., and Claiborne, A. (1997) Cloning and sequencing of two enterococcal *glpK* genes and regulation of the encoded glycerol kinases by phosphoenolpyruvate-dependent, phosphotransferase system-catalyzed phosphorylation of a single histidyl residue, *J. Biol. Chem. 272*, 14166−14174.
14. Otwinowski, Z., and Minor, W. (1997) Processing of X-ray Diffraction Data Collected in Oscillation Mode, *Methods Enzymol. 276*, 307−326.
15. Collaborative Computational Project, Number 4 (1994) *Acta Crystallogr. D50*, 760−763.
16. Brünger, A. T. (1993) *X-PLOR version 3.1. A System for X-ray crystallography and NMR*, Yale University Press, New Haven, CT.
17. Tong, L., and Rossman, M. G. (1997) Rotation Function Calculations with GLRF Program, *Methods Enzymol. 276*, 594−610.
18. Navaza, J., and Saludjian, P. (1997) AmoRe: An Automated Molecular Replacement Program Package, *Methods Enzymol. 276*, 581−593.
19. Kissinger, C. R., Gehlhaar, D. K., and Fogel, D. B. (1999) Rapid automated molecular replacement by evolutionary search, *Acta Crystallogr. D55*, 484−491.
20. Cowtan, K. (1994) DM: An automated procedure for phase improvement by density modification, *Joint CCP4 and ESF-EACBM Newsletter on Protein Crystallography 31*, 34−38.
21. Read, R. J. (1986) Improved Fourier coefficients for maps using phases from partial structures with errors, *Acta Crystallogr. A42*, 140−149.
22. Liu, W. Z., Faber, R., Feese, M., Remington, S. J., and Pettigrew, D. W. (1994) *Escherichia coli* glycerol kinase: role of a tetramer interface in regulation by fructose 1,6-bisphosphate and phosphotransferase system regulatory protein III^{Glc}, *Biochemistry 33*, 10120−10126.
23. Doublie, S. (1997) Preparation of Selenomethionyl Proteins for Phase Determination, *Methods Enzymol. 276*, 530−537.
24. Terwilliger, T. (2002) Automated structure solution, density modification, and model building, *Acta Crystallogr. D58*, 1937−1940.
25. Jones, T. A. (1978) A graphics model building and refinement system for macromolecules, *J. Appl. Crystallogr. 11*, 268−272.
26. Yeh, J. I. (2003) A Manual Nanoscale Crystallization Method, *Acta Crystallogr. D59*, 1408−1413.
27. Kleywegt, G. J., and Brünger, A. T. (1996) Checking your imagination: applications of the free R value, *Structure 4*, 897−904.
28. Kleywegt, G. J. (2000) Validation of protein crystal structures, *Acta Crystallogr. D56*, 249−265.
29. Kleywegt, G. J. (1999) Experimental assessment of differences between related protein crystal structures, *Acta Crystallogr. D55*, 1878−1884.
30. Anderson, C. M., Stenkamp, R. E., McDonald, R. C., and Steitz, T. A. (1978) A refined model of sugar binding site of yeast hexokinase, *J. Mol. Biol. 123*, 207−219.
31. Bystrom, C. E., Pettigrew, D. W., Branchaud, B. P., O'Brien, P., and Remington, S. J. (1999) Crystal structures of *Escherichia coli* glycerol kinase variant S58 → W in complex with nonhydrolyzable ATP analogues reveal a putative active conformation of the enzyme as a result of domain motion, *Biochemistry 38*, 3508−3518.
32. Darbon, E., Servant, P., Poncet, S., and Deutscher, J. (2002) Antitermination by GlpP, catabolite repression via CcpA, and inducer exclusion triggered by P∼GlpK dephosphorylation control *Bacillus subtilis glpFK* expression, *Mol. Microbiol. 43*, 1039−1052.
33. Bennett, W. S., Jr., and Steitz, T. A. (1980) Structure of a complex between yeast hexokinase and glucose. II. Detailed comparison of conformation and active site configuration with the native hexokinase B monomer and dimer, *J. Mol. Biol. 140*, 211−230.
34. Knowles, J. R. (1980) Enzyme-catalyzed phosphoryl transfer reactions, *Annu. Rev. Biochem. 49*, 877−919.
35. Wang, G., Sondej, M., Garrett, D. S., Peterkofsky, A., and Clore, G. M. (2000) A common interface on histidine-containing phosphocarrier protein for interaction with its partner proteins, *J. Biol. Chem. 275*, 16401−16403.
36. Chen, Y., Reizer, J., Saier, M. H., Jr., Fairbrother, W. J., and Wright, P. E. (1993) Mapping of the binding interfaces of the proteins of the bacterial phosphotransferase system, HPr and IIA^{Glc}, *Biochemistry 32*, 32−37.
37. Garrett, D. S., Seok, Y. J., Peterkofsky, A., Clore, G. M., and Gronenborn, A. M. (1997) Identification by NMR of the binding surface for the histidine-containing phosphocarrier protein HPr on the N-terminal domain of enzyme I of the *Escherichia coli* phosphotransferase system, *Biochemistry 36*, 4393−4398.
38. Wehtje, C., Beijer, L., Nilsson, R. P., and Rutberg, B. (1995) Mutations in the glycerol kinase gene restore the ability of a

ptsGHI mutant of *Bacillus subtilis* to grow on glycerol, *Microbiology 141*, 1193−1198.
39. Gonzy-Treboul, G., de Waard, J. H., Zagorec, M., and Postma, P. W. (1991) The glucose permease of the phosphotransferase system of *Bacillus subtilis*: evidence for II^{Glc} and III^{Glc} domains, *Mol. Microbiol. 5*, 1241−1249.
40. Beijer, L., and Rutberg, L. (1992) Utilisation of glycerol and glycerol 3-phosphate is differently affected by the phosphotransferase system in *Bacillus subtilis*, *FEMS Microbiol. Lett. 79*, 217−220.

BI034258O